Two-Headed Binding of the Unphosphorylated Nonmuscle Heavy Meromyosin·ADP Complex to Actin

Mihály Kovács,[‡] Judit Tóth,[‡,§] László Nyitray,[§] and James R. Sellers*[,‡]

Laboratory of Molecular Cardiology, National Heart, Lung and Blood Institute, National Institutes of Health, Bethesda, Maryland 20892-1762, and Department of Biochemistry, Eötvös Loránd University, Pázmány P. sétány 1/C, H-1117 Budapest, Hungary

Received November 10, 2003; Revised Manuscript Received January 27, 2004

ABSTRACT: The enzymatic and motor function of smooth muscle and nonmuscle myosin II is activated by phosphorylation of the regulatory light chains located in the head portion of myosin. Dimerization of the heads, which is brought about by the coiled-coil tail region, is essential for regulation since single-headed fragments are active regardless of the state of phosphorylation. Utilizing the fluorescence signal on binding of myosin to pyrene-labeled actin filaments, we investigated the interplay of actin and nucleotide binding to thiophosphorylated and unphosphorylated recombinant nonmuscle IIA heavy meromyosin constructs. We show that both heads of either thiophosphorylated or unphosphorylated heavy meromyosin bind very strongly to actin (K_d < 10 nM) in the presence or absence of ADP. The heads have high and indistinguishable affinities for ADP (K_d around 1 μM) when bound to actin. These findings are in line with the previously observed unusually loose coupling between nucleotide and actin binding to nonmuscle myosin IIA subfragment-1 (Kovács et al. (2003) *J. Biol. Chem. 278*, 38132.). Furthermore, they imply that the structure of the two heads in the ternary actomyosin−ADP complex is symmetrical and that the asymmetrical structure observed in the presence of ATP and the absence of actin in previous investigations (Wendt et al. (2001) *Proc. Natl. Acad. Sci. U.S.A. 98*, 4361) is likely to represent an ATPase intermediate that precedes the actomyosin−ADP state.

Myosins are a large and diverse superfamily of actin-dependent molecular motors, in which a wide variety of regulatory mechanisms has developed to control enzymatic activity and motor function. Regulation can involve accessory proteins on the actin filament, like the troponin−tropomyosin and calponin−caldesmon systems in different vertebrate muscle types (*1*, *2*). Alternatively, in some myosins, control of activity can be brought about by changes in the myosin holoenzyme itself, by the binding of Ca^{2+} to a myosin light chain or calmodulin or by reversible phosphorylation of the heavy or light chains (*3*).

Nonmuscle myosin II, like all other conventional myosins, is composed of two identical heavy chains forming the motor, neck, and tail domains with each heavy chain having an essential (ELC)[1] and a regulatory (RLC) light chain attached to its neck region. The N-terminal motor domain confers enzymatic activity, and together with the neck region, it forms the "head" portion of myosin (subfragment-1, S1). The heavy chains dimerize by formation of a coiled-coil structure in the C-terminal tail domain.

Vertebrate nonmuscle and smooth muscle myosin IIs share the common feature that their ATPase and motile activity is turned on by RLC phosphorylation (*4*). In regulated myosin IIs, single-headed (S1) fragments are constitutively active (*5*). In contrast, double-headed heavy meromyosin (HMM) constructs containing a portion of the coiled-coil tail exhibit normal regulation (*5*−*7*). This implies that interaction between the two heads is required for formation of the *off*-state of myosin. This assumption is strengthened by biochemical studies (*6*, *7*) and also by electron microscopic image reconstructions, in which one head of unphosphorylated smooth muscle HMM is bent toward the other in a way that its actin binding site interacts with the so-called converter region of the other head (*8*−*10*). The latter region is a key element in force production that is in feedback with the ATPase site (*11*), and thus, this structure provides a ready explanation of how the actin-activated ATPase activity of either head is inhibited. This asymmetrical structure was obtained in the absence of actin and in the presence of ATP, and it was observed only in the unphosphorylated state. The contents of the active site of each head are unknown, and it is also not clear in which ATPase intermediate state the myosin heads are trapped.

Pyrene-labeled actin filaments show a large quench in fluorescence on binding to various myosin isoforms both in

* To whom correspondence should be addressed. Mailing address: Laboratory of Molecular Cardiology, National Heart, Lung and Blood Institute, National Institutes of Health, Building 10, Room 8N202, Bethesda, MD 20892-1762. Tel: 301-496-6887. Fax: 301-402-1542. E-mail: sellersj@nhlbi.nih.gov.

[‡] National Institutes of Health.

[§] Eötvös Loránd University.

[1] Abbreviations: ATPγS, adenosine-5′-*O*-3-thiotriphosphate; DTT, dithiothreitol; EDTA, ethylenediamine tetraacetic acid; EGTA, ethylene glycol bis (β-aminoethyl ether)-*N*,*N*,*N*′,*N*′-tetraacetic acid; ELC, essential light chain; HMM, heavy meromyosin; k_{obs}, observed rate constant; mant, 2′(3)-*O*-(*N*-methylanthraniloyl); MLCK, myosin light chain kinase; MOPS, 4-morpholinepropanesulfonic acid; NM, nonmuscle; PAGE, polyacrylamide gel electrophoresis; RLC, regulatory light chain; S1, subfragment-1; *tP*, thiophosphorylated; Tris, tris-hydroxymethyl-aminomethane; *uP*, unphosphorylated.

10.1021/bi036007l CCC: $27.50
Published on Web 03/19/2004

the absence of nucleotide and in the presence of ADP that has been extensively utilized in solution kinetic studies (*12*). Such investigations of the ternary complex of smooth muscle HMM with actin and ADP have led to conflicting conclusions. Berger et al. (*13*) found that upon ADP binding, the structure of unphosphorylated recombinant smooth muscle HMM becomes asymmetrical and only one of the heads can bind to actin, which results in a reduced amplitude of pyrene fluorescence change on actomyosin interaction compared to the phosphorylated state. Conversely, the experiments of Ellison et al. (*14*) on tissue-purified proteolytic material showed symmetrical two-headed actin binding of the smooth muscle HMM·ADP complex, regardless of the state of phosphorylation.

On the basis of available data, it seems that the structural and kinetic basis of phosphorylation-dependent regulation of smooth muscle and nonmuscle myosins is very similar (*3*). The unphosphorylated off-state of nonmuscle myosin II may play an important role in prolonged tension maintenance in both smooth muscle and nonmuscle cells. Therefore, it is of great interest to determine how the nucleotide bound in the active site affects the actin-binding properties of the unphosphorylated myosin heads.

To address this problem, we characterized the actin and ADP interaction of a human nonmuscle IIA (NMIIA) HMM fragment produced in the baculovirus−Sf9 expression system. The analysis of pyrene-actin fluorescence transients shows that both thiophosphorylated and unphosphorylated NMIIA HMM bind strongly to actin with both heads, regardless of the presence of ADP. We also find that the two heads have high and indistinguishable ADP affinities when bound to actin. These results show that there is a loose coupling between actin and ADP binding in NMIIA HMM and imply that the two heads, either phosphorylated or unphosphorylated, have a similar interaction with and affinity for actin in the ternary actomyosin·ADP complex. On the basis of spectroscopic and kinetic arguments, we propose that the asymmetrical off-state structure seen in ATP in the absence of actin in electron microscopic image reconstruction studies (*8*−*10*) represents an intermediate that is different from the actomyosin·ADP state.

EXPERIMENTAL PROCEDURES

Protein Expression and Purification. In this study, we used a recombinant construct that contains the first 1337 amino acids of the human nonmuscle myosin IIA (NMIIA) heavy chain, resembling heavy meromyosin (HMM). A C-terminal FLAG-tag (sequence DYKDDDDK) was appended to the construct to aid affinity purification. The recombinant NMIIA HMM heavy chain was coexpressed with light chains (bovine nonmuscle MLC_{17B} and chicken nonmuscle MLC_{20}) in the baculovirus−Sf9 expression system. Cloning, expression, and preparation of NMIIA HMM was described earlier (*15*).

Actin was prepared from rabbit skeletal muscle according to Spudich and Watt (*16*) and pyrene-labeled as described in Cooper et al. (*17*). ATPγS was from Roche Applied Science (Indianapolis, IN). Pyrene iodoacetamide was purchased from Molecular Probes (Eugene, OR). Phalloidin was from Calbiochem (La Jolla, CA). Other chemicals were from Sigma.

HMM concentrations stated throughout this article are expressed in terms of myosin heads.

RLC Thiophosphorylation. Thiophosphorylation of the RLC (in 5−10 μM NMIIA HMM solutions) was performed essentially as described by Facemyer and Cremo (*18*) in the presence of 10 mM MOPS (pH 7.2), 3 mM NaN_3, 50 mM NaCl, 2.5 mM $MgCl_2$, 2.5 mM $CaCl_2$, 1 mM ATPγS, 0.25 μM calmodulin, and 4 μg/mL MLCK. The mixture was incubated at 25 °C for 1 h. Thiophosphorylated NMIIA HMM was made nucleotide free by gel filtration on a 5-mL Sephadex G-50 column.

The phosphorylation state of the light chains was verified by gel electrophoresis using glycerol (40%)/polyacrylamide (11%) gels (*19*). Samples of 10 μg of HMM were loaded in a buffer containing 8 M urea, 10 mM DTT, 0.2 mM EDTA, and 33 mM Tris-glycine (pH 8.6) and run at 10 mA for 2 h.

Kinetic Assays. Steady-state ATPase activities were measured at 25 °C by a NADH-coupled assay as described earlier (*20*) in a low ionic strength buffer (10 mM MOPS (pH 7.0), 2 mM $MgCl_2$, 0.15 mM EGTA, 1 mM ATP, 40 units/mL lactate dehydrogenase, 200 units/mL pyruvate kinase, 1 mM phosphoenolpyruvate, and 200 μM NADH).

All stopped-flow measurements were carried out in a KinTek SF-2001 instrument (KinTek Corp., Austin, TX) at 25 °C in a buffer comprising 20 mM MOPS (pH 7.0), 5 mM $MgCl_2$, 0.1 mM EGTA, and 100 mM KCl. Pyrene fluorescence was excited at 365 nm (6 nm band-pass), and emission was monitored through a 400 nm long-pass cutoff filter. Typically, 4−12 traces were averaged for data analysis.

Single ATP turnovers by NMIIA HMM were also followed in a SPEX FluoroMax3 spectrofluorometer at 25 °C in a buffer comprising 10 mM MOPS (pH 7.1), 1 mM $MgCl_2$, 0.1 mM EGTA, and 3 mM NaN_3. In these experiments, pyrene was excited at 344 nm (0.5 nm band-pass), and emission detected through a monochromator centered at 406 nm.

Pyrene photobleaching controls were recorded and used for correction of long time scale (>10 s) stopped-flow and conventional spectrofluorometer records. Before analysis of amplitudes, the background signal level measured with assay buffer only was subtracted from all fluorescence records.

Pyrene-actin was stabilized in all experiments by the addition of an equimolar amount of phalloidin. NMIIA HMM was made ADP free by incubation with 0.01 unit/mL apyrase at 25 °C for 30 min.

Data were analyzed using the KinTek SF-2001 software and Microcal Origin v6.0 (Microcal Software). Means and standard errors reported are generally those of two or three rounds of experiment.

In stopped-flow-based titration experiments, the concentrations of the reactants before mixing are relevant in terms of analyzing reaction amplitudes, whereas the rate parameters reflect concentrations after the mix. To avoid confusion, we specify at the introduction of each experiment whether premixing or postmixing concentrations are stated.

Titration curves of actin binding were analyzed according to the method of Kurzawa and Geeves (*21*) except that both the maximal fluorescence change and the concentration of the titrated species (i.e., pyrene-actin) were left free to float during the fitting iterations.

RESULTS

Thiophosphorylation of NMIIA HMM. We expressed a two-headed, HMM-like construct of nonmuscle myosin IIA

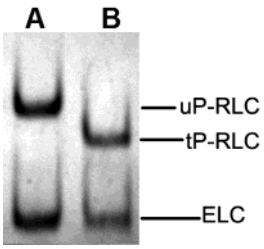

FIGURE 1: Thiophosphorylation of the RLC. Glycerol−urea−PAGE electrophoretogram of the light chains is shown. In lane A, baculovirus-expressed NMIIA HMM had fully unphosphorylated RLCs (*uP*-RLC) as isolated. In lane B, the RLCs of NMIIA HMM after incubation with MLCK and ATPγS were fully thiophosphorylated (*tP*-RLC), as seen from the higher mobility of this species compared to *uP*-RLC. The ELCs were unaffected by MLCK treatment.

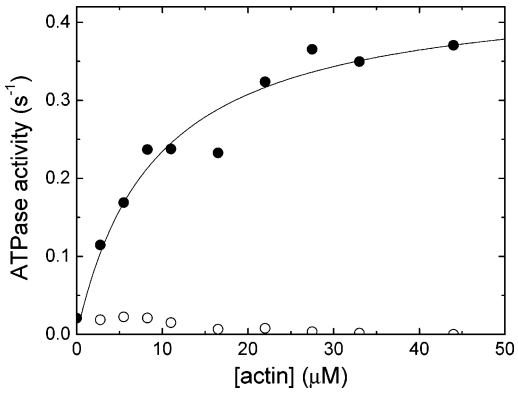

FIGURE 2: ATPase activity of *tP*-HMM and *uP*-HMM. Steady-state MgATPase activity of *tP*-HMM (●) and *uP*-HMM (○) was measured by a NADH-coupled assay. *tP*-HMM had a basal ATPase activity of 0.013 ± 0.04 s^{-1}, which was activated by actin to a V_{max} of 0.45 ± 0.03 s^{-1}, and a K_{ATPase} of 9 ± 2 μM (hyperbolic fit of the dataset is shown). *uP*-HMM had no detectable actin activation of its ATPase activity. Conditions were 25 °C, 10 mM MOPS (pH 7.0), 2 mM $MgCl_2$, 0.15 mM EGTA, and 1 mM ATP.

in the baculovirus−Sf9 system. Generally, 3−5 mg of FLAG-tagged protein could be prepared from about 4×10^9 cells.

To study the effect of light chain phosphorylation on myosin function, the RLC was thiophosphorylated by myosin light chain kinase (MLCK) using adenosine-5′-*O*-3-thiotriphosphate (ATPγS), a structural analogue of ATP, as a substrate (*18*). To the limit of electrophoretic detectability, the regulatory light chain (RLC) of the recombinant NMIIA HMM construct purified from the cells was fully in the unphosphorylated form (Figure 1). Treatment with alkaline phosphatase did not have an effect on the glycerol−PAGE pattern of the light chains (data not shown). The RLC could be fully thiophosphorylated by treatment with MLCK, and only a single RLC band was detectable after the treatment (Figure 1).

Effect of Phosphorylation on ATPase Activity. The quality of phosphorylation-dependent regulation of the NMIIA HMM construct was assessed by steady-state and single turnover ATPase measurements. In the thiophosphorylated form, NMIIA HMM showed a low basal steady-state ATPase activity (0.021 ± 0.003 s^{-1}) that was activated by actin to a V_{max} of 0.45 ± 0.03 s^{-1}, with half-saturation at 9 ± 2 μM actin concentration (Figure 2). Compared to an NMIIA S1 construct characterized earlier (*22*), the maximal actin-activated ATPase activity of NMIIA HMM is significantly higher ($V_{max} = 0.17 \pm 0.005$ s^{-1} in S1 and 0.45 ± 0.03 s^{-1} in *tP*-HMM) and the K_{ATPase} value is lower by an order of magnitude (72 ± 4 μM in S1 and 9 ± 2 μM in *tP*-HMM, see also in Table 1). This kind of difference between single-headed and double-headed forms is also observed in smooth muscle myosin (*23*, *24*).

In contrast to *tP*-HMM, the unphosphorylated form did not show measurable actin activation of the ATPase activity (Figure 2). The low activity of *uP*-HMM was confirmed by single turnover experiments (Table 1), which are more suitable for determination of very low ATPase activities where the background signal change introduces a large error into the linear steady-state slope obtained (*25*). From the results it appears that the conditions used are suitable for production of practically 100% on- and off-state form of NMIIA-HMM.

Kinetic Model of the Interaction of NMIIA HMM with Actin and Nucleotides. A simplified kinetic model shown in Scheme 1 was sufficient for the interpretation of the transient kinetic results obtained in this study. In this model, ADP and actin binding to the myosin head are treated as single-step reactions. Upon ATP binding to actomyosin, the initial second-order collision step (K_1) is followed by an irreversible isomerization (k_2) that limits the observed rate constant of ATP-induced actomyosin dissociation at high ATP concentrations. This step is followed by a rapid detachment of the myosin·ATP complex from actin.

Dissociation of the Acto-uP-HMM Complex by ATP. Population of the weak actin binding states by *uP*-HMM was monitored by rapidly mixing 0.05 μM pyrene-actin and 0.1 μM *uP*-HMM (in heads, postmix concentrations stated) with a range of ATP concentrations. The dependence of the observed rate constant of pyrene fluorescence increase was hyperbolic with a maximal k_{obs} of 230 ± 6 s^{-1} (corresponding to k_2) and half-saturation (K_1) at 980 ± 50 μM ATP (Figure 3). Linear fit to the data points at low ATP concentration (up to 50 μM) gave an apparent second-order binding constant of ATP to actomyosin (k_2/K_1) of 0.23 ± 0.02 μM^{-1} s^{-1} (Figure 3, inset). These parameters are very similar to those obtained with NMIIA S1 in our previous study (*22*, Table 1). Throughout the examined ATP concentration range, a minor (<10%) slow phase with a k_{obs} of 1.5−3 s^{-1} was present that we attribute to the presence of residual small amounts of ADP in protein or ATP stock solutions or both.

Actin Interaction of tP- and uP-HMM in the Presence and Absence of ADP. The interaction of HMM with actin was assessed by a stopped-flow technique in which 0.075 μM pyrene-actin was premixed with a range of HMM concentrations and the equilibrium binding mixtures were rapidly mixed with 300 μM ATP (premixing concentrations stated). Assuming that ATP causes complete dissociation of HMM from pyrene-actin, the amplitude of the observed pyrene fluorescence transient will reflect the concentration of the strongly bound pyrene-acto-HMM complex before mixing. The experiment was performed both with *tP*-HMM and *uP*-HMM in the absence and presence of 50 μM ADP.

In the case of *tP*-HMM, the transients showed a major phase with a k_{obs} around 40 s^{-1} in the absence of ADP (Figure 4A), corresponding to ATP-induced dissociation of the acto-*tP*-HMM rigor complex. The minor slow phase mentioned

Table 1: Rate and Equilibrium Parameters of Fragments of Phosphorylation-Regulated Myosins[a]

	nonmuscle IIa			smooth muscle		
	S1[b]	*tP*-HMM[c]	*uP*-HMM[c]	S1	*tP*-HMM	*uP*-HMM
ATPase Activity						
basal (s^{-1})	0.013 ± 0.004	0.021 ± 0.003		0.06[d]		
V_{max} (s^{-1})	0.17 ± 0.005	0.45 ± 0.03		0.7−1.8[d,e]	1.9−2.5[e,f]	
k_{ST} (s^{-1})[g]			0.0012			0.002[h]
K_{ATPase} (μM)	72 ± 4	9 ± 2		60−100[d,e]	20−40[e,f]	
ATP-Induced Actomyosin Dissociation[i]						
K_1 (μM)	~900		980 ± 50			
k_2 (s^{-1})	~190		230 ± 6			
k_2/K_1 (μM^{-1} s^{-1})	0.21 ± 0.04	~0.25	0.23 ± 0.02	0.47		
Actin Interaction[i]						
K_A (μM)	<0.01	<0.01	<0.01			
K_{DA} (μM)	~0.02	<0.01	<0.01	0.049 ± 0.028[j,k]	0.018 ± 0.004[k,l]	0.051 ± 0.010[k,l]
ADP Interaction						
k_D (s^{-1})	0.8 ± 0.3[m]		5.0 ± 1.8; 0.7 ± 0.1 (bp)[m,n]	1.9 [j]	3 [l]	2.4[l]
k_{AD} (s^{-1})	2.2 ± 0.5	7.3 ± 0.6; 1.2 ± 0.1 (bp)	2.6 ± 0.2; 0.8 ± 0.1 (bp)	22 [j]	~40[l]	~50[l]
K_{AD} (μM)	1.1 ± 0.3	2.2 ± 0.8	1.3 ± 0.2	5.0[j]	10 [l]	1−2; 10−20[l,o]

[a] bp, biphasic. Nomenclature of steps refers to Scheme 1. [b] Reference *22*. [c] Present study. [d] Reference *32*. [e] Reference *33*. [f] Reference *29*. [g] Single turnover rate constant of *uP*-HMM in the presence of actin (independent of actin concentration). [h] Reference *25*. [i] Pyrene-actin. [j] Reference *34*. [k] In 200 mM KCl. [l] Reference *13*. [m] mantADP. [n] Determined by following mant fluorescence change on mixing 0.5 μM *uP*-HMM (in heads) and 2 μM mantADP with 150 μM ATP (conditions the same as those in Figure 3). [o] Different ADP affinities of the two heads were detected.

Scheme 1 [a]

$$\begin{array}{ccccccc} & & \overset{K_{AD}}{} & & \overset{K_1}{} & & \overset{k_2}{} \\ \mathrm{AMD} & \rightleftharpoons & \mathrm{AM} & \rightleftharpoons & \mathrm{AMT} & \rightarrow & \mathrm{A\text{-}MT} \rightarrow \mathrm{A} + \mathrm{MT} \\ K_{DA}\,\Downarrow & & \Downarrow K_A & & & & \\ \mathrm{MD} & \underset{K_D}{\rightleftharpoons} & \mathrm{M} & & & & \end{array}$$

[a] Symbols used: A, actin; M, myosin (S1 or HMM); T, ATP; D, ADP. All equilibrium constants are expressed as dissociation constants. Rate constants are denoted as k_i and k_{-i} in the dissociation and association directions, respectively. Additional arrows for associating and dissociating components are omitted for clarity.

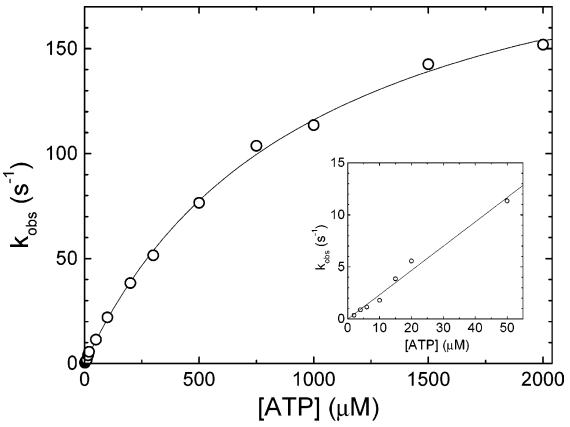

FIGURE 3: ATP-induced dissociation of acto-*uP*-HMM. The observed rate constants of the pyrene fluorescence transients upon mixing 0.05 μM pyrene-actin and 0.1 μM *uP*-HMM (in heads, postmix concentrations) with ATP are plotted against ATP concentration. The solid line is a hyperbolic fit with a maximal k_{obs} of 230 ± 6 s^{-1} (corresponding to k_2) and half-saturation (K_1) at 980 ± 50 μM ATP. In the inset, a linear fit of the data points at low ATP concentration yielded an apparent ATP on-rate constant (k_2/K_1) of 0.23 ± 0.02 μM^{-1} s^{-1}. Conditions were 25 °C, 20 mM MOPS (pH 7.0), 5 mM $MgCl_2$, 0.1 mM EGTA, and 100 mM KCl.

in the previous section was also present in these experiments. A longer preincubation of the pyrene-acto-HMM mixture with 0.01 units/ml apyrase (2 h at 25 °C) reduced the amplitude of this phase, which indicates that it may originate from residual ADP in protein preparations.

In the presence of 50 μM ADP, the rate constant of acto-*tP*-HMM dissociation was limited by the ADP dissociation process (k_{AD}). The observed pyrene fluorescence transients were best described by two exponentials with k_{obs} values of 7.3 ± 0.6 and 1.2 ± 0.1 s^{-1} (Figure 4A). The ratio of the amplitudes of the two phases remained constant throughout the HMM concentration range examined (about 40% fast phase and 60% slow phase, cf. Figure 4B).

Figure 4B shows the dependence of the amplitudes of the pyrene fluorescence change (expressed as $\Delta F/F_{final}$, where F_{final} is the fluorescence level of detached pyrene-actin) on *tP*-HMM concentration. These titration curves show that *tP*-HMM binds very tightly to actin both in the absence and presence of ADP with a dissociation constant much lower than the pyrene-actin concentration used in the experiments (K_A, K_{DA} < 0.01 μM). The amplitudes of both phases of the ADP transients show similar tight binding. It is also apparent that ADP does not have an effect on the maximal amplitude of the change (0.90 ± 0.05 in the absence, and 0.91 ± 0.05 in the presence of ADP), which indicates a similar mode of *tP*-HMM binding to actin regardless of the presence of ADP.

uP-HMM showed a similar behavior to *tP*-HMM in these experiments (Figure 4C,D). In the absence of ADP, the fast rate constant of dissociation was around 40 s^{-1} with a similar minor phase as that in *tP*-HMM. The transients in 50 μM ADP were biexponential with rate constants of 2.6 ± 0.2 s^{-1} (70% of total amplitude) and 0.8 ± 0.1 s^{-1} (30% of total amplitude) (Figure 4C). Similar to *tP*-HMM, *uP*-HMM showed tight actin binding both in the absence and presence of ADP (Figure 4D). Importantly, ADP did not have a large effect on the maximal amplitude of the pyrene fluorescence change. Indeed, the change in the presence of ADP (0.76 ± 0.10) was somewhat larger than in its absence (0.63 ± 0.05). Even though the maximal amplitudes in *uP*-HMM are smaller than those in *tP*-HMM (see below), the results imply

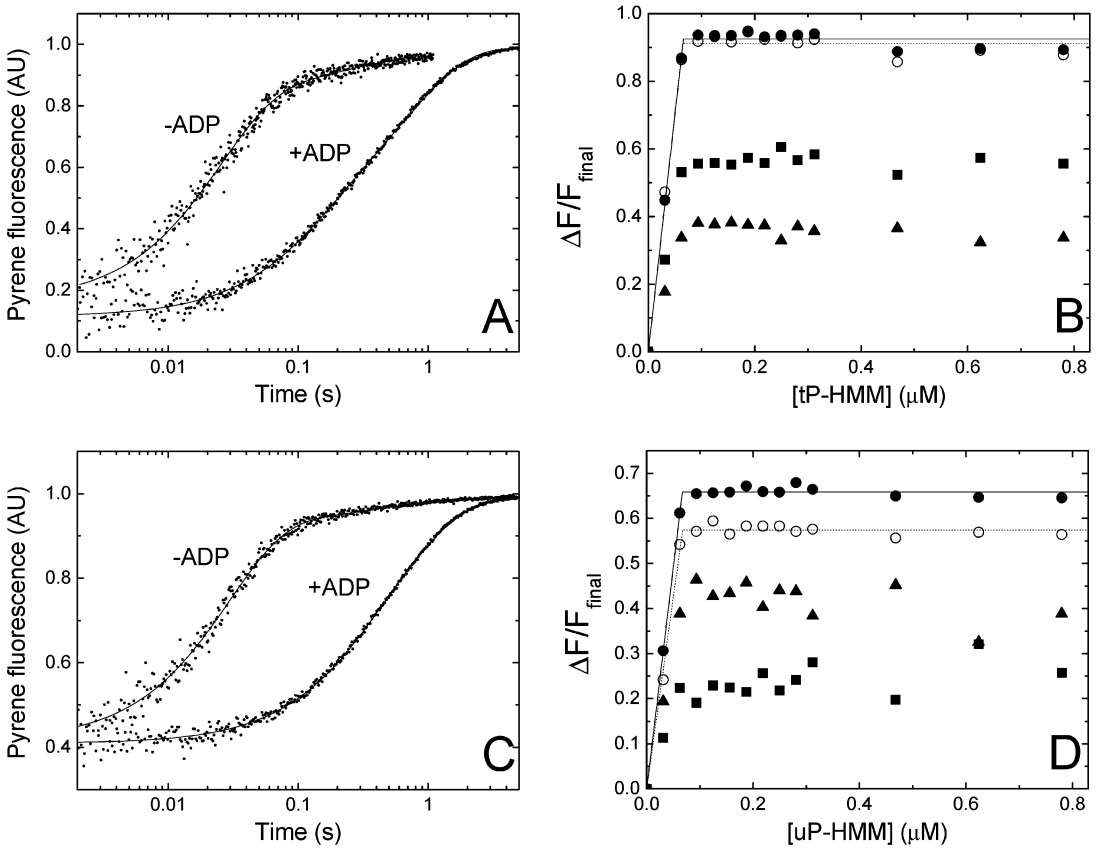

FIGURE 4: Interaction of *tP*-HMM and *uP*-HMM with actin in the presence and absence of ADP. Panel A shows pyrene fluorescence transients of the ATP-induced dissociation of acto-*tP*-HMM (−ADP trace) or acto-*tP*-HMM·ADP (+ADP trace) complex. Pyrene-actin (0.1 μM) was manually premixed with 0.6 μM *tP*-HMM (in heads) in the absence or presence of 50 μM ADP and then rapidly mixed with 300 μM ATP in the stopped-flow (concentrations before rapid mixing stated throughout this figure). The k_{obs} of the reaction was 41 s^{-1} in the absence of ADP with a minor (10% amplitude) 4.5 s^{-1} phase in the trace shown. In ADP, the transient was also biphasic with rate constants of 8.0 and 1.3 s^{-1} (k_{AD}). Note the logarithmic time scale in panels A and C. Panel B shows the dependence of the total amplitude of the reaction on *tP*-HMM concentration in the presence (●) and absence (○) of 50 μM ADP. The solid lines are fitted binding curves with very low K_d (K_A, K_{DA} < 0.01 μM, see also in Materials and Methods). The maximal relative fluorescence change (expressed as $\Delta F/F_{final}$, where F_{final} is the fluorescence level of detached pyrene-actin) was 0.92 in the presence and 0.91 in the absence of ADP in the experiment shown. Amplitudes of the fast (▲) and slow (■) phases of the +ADP transients are also shown. HMM concentrations are expressed in terms of myosin heads. Panel C shows ATP-induced dissociation of acto-*uP*-HMM (−ADP trace) and acto-*uP*-HMM·ADP (+ADP trace) under the same experimental conditions as those in panel A. In the absence of ADP, k_{obs} of the reaction was 34 s^{-1} with a minor phase (10% amplitude) of 2.0 s^{-1} in the experiment shown. In 50 μM ADP, the observed rate constants of the biphasic transient were 3.1 and 1.0 s^{-1} (k_{AD}). Panel D shows the dependence of the total amplitude on *uP*-HMM concentration in the presence (●) and absence (○) of 50 μM ADP. The fitted maximal relative fluorescence changes in the presence and absence of ADP were 0.66 and 0.57, respectively, in the experiment shown. Fast (▲) and slow (■) phase amplitudes of the +ADP traces are also shown. Conditions were the same as those in Figure 3.

that nonmuscle HMM in the dephosphorylated state binds to actin in a double-headed manner regardless of the presence of ADP. This behavior is similar to that reported by Ellison et al. for smooth muscle myosin (*14*), contrasting to the findings of Berger et al. (*13*).

ADP Affinity of Acto-tP-HMM and Acto-uP-HMM Complexes. We investigated the ADP affinity of the acto-HMM complex by preincubating 0.05 μM pyrene-actin and 0.075 μM *tP*-HMM or *uP*-HMM (in heads) with various concentrations of ADP (0.01−100 μM), and then rapidly mixing this equilibrium mixture with 300 μM ATP (premixing concentrations stated). The obtained pyrene fluorescence transients were biphasic in most cases. The fast phase represents the fraction of acto-HMM not bound to ADP and therefore undergoing rapid dissociation upon mixing with ATP. The slow phase reflects the ADP-bound fraction of acto-HMM, in which ADP release will limit the kinetics of acto-HMM dissociation.

Figure 5A shows representative transients of acto-*tP*-HMM dissociation at different ADP concentrations. The k_{obs} values of the fast and slow phases phase were 35 ± 4 and 3.8 ± 0.5 s^{-1}, respectively, and they did not depend on ADP concentration. The k_{obs} of the slow phase falls between the observed rate constants of the biphasic ADP release transients of Figure 4. In the ADP titration experiments, we treated this process as a single exponential to aid determination of the ADP dissociation constants. The total amplitude of the pyrene fluorescence change was also constant within the ADP concentration range studied. The fractional amplitudes of the fast and slow phases, however, showed hyperbolical dependence on ADP concentration with the fast phase being predominant at low ADP concentration, whereas at high ADP concentration, the transients consisted solely of the slow phase (Figure 5B). Hyperbolic fits of the amplitude data of both phases gave similar K_{AD} values (2.2 ± 0.8 μM). The phenomenon that the fractional amplitude of the slow phase

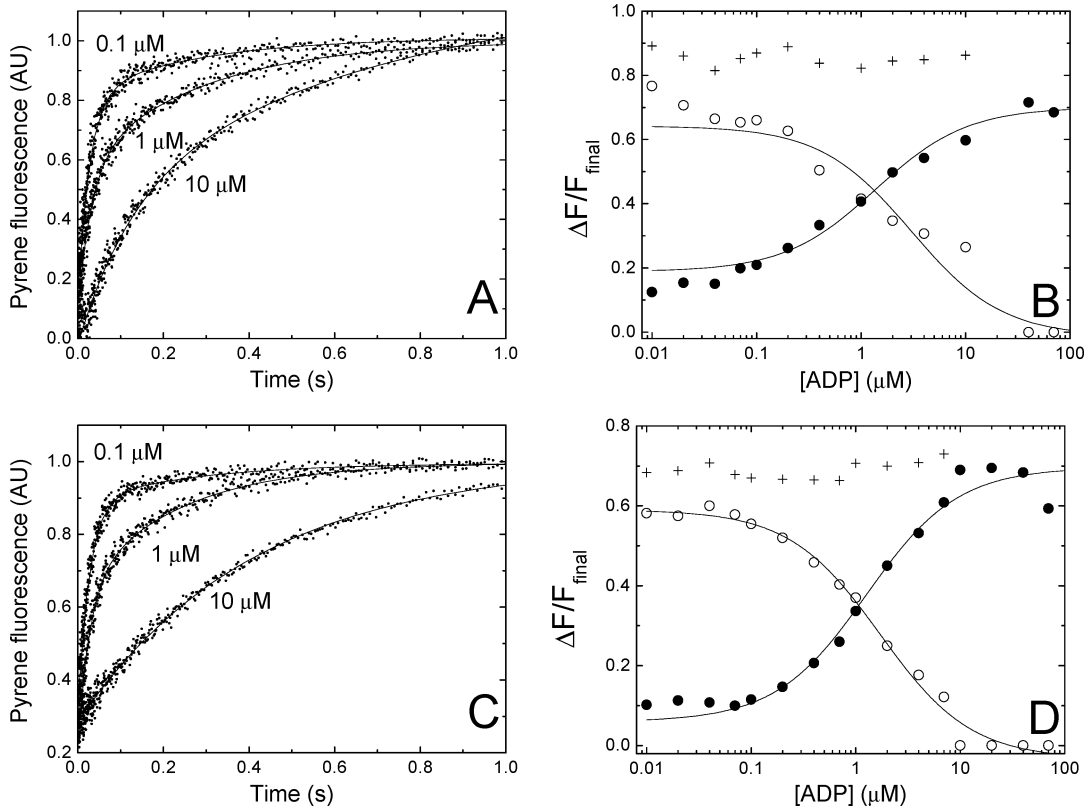

FIGURE 5: ADP affinity of acto-*tP*-HMM and acto-*uP*-HMM. In panel A, 0.075 μM *tP*-HMM (in heads) was preincubated with 0.05 μM pyrene-actin and the indicated ADP concentrations and then rapidly mixed with 300 μM ATP in the stopped-flow (premixing concentrations stated). The observed transients were biphasic with observed rate constants of 35 ± 4 s^{-1} (representing the dissociation of acto-*tP*-HMM by ATP) and 3.8 ± 0.5 s^{-1} (representing the ADP-bound fraction of acto-*tP*-HMM where acto-HMM dissociation is limited by ADP release). Panel B shows the dependence of the total amplitude (+, cf. Figure 4B) and the amplitudes of the fast (○) and slow (●) phases on ADP concentration. The total amplitude was constant over the ADP concentration range studied, whereas the fast and slow phases showed a hyperbolic dependence on ADP concentration, yielding a K_{AD} of 2.2 ± 0.8 μM. (Data points below 0.2 μM ADP concentration were omitted from the hyperbolic fits in panels B and D.) Panel C shows pyrene fluorescence transients of the dissociation of the acto-*uP*-HMM complex in the presence of the indicated ADP concentrations under the same conditions as those in panel A. The rate constants of the two phases were 35 ± 5 and 3.5 ± 0.8 s^{-1}. Panel D shows the ADP concentration dependence of the total amplitude (+) and the amplitudes of the fast (○) and slow (●) phases. Hyperbolic fits to the fast and slow phase amplitudes gave a K_{AD} of 1.3 ± 0.2 μM. Conditions were the same as those in Figure 3.

does not converge to zero with lowering ADP concentration can arise from small amounts of contaminating ADP in the proteins as seen also in other experiments described above. The data points below 0.2 μM ADP were omitted from the hyperbolic fits.

The transients in *uP*-HMM were also biphasic in most part of the ADP concentration range studied with k_{obs} values of 35 ± 5 and 3.8 ± 0.9 s^{-1}. Representative traces are shown in Figure 5C. The total amplitude of the fluorescence change was independent of ADP concentration, and it was significantly lower than that in *tP*-HMM (Figure 5D), consistent with the results of the experiments in Figure 4. The fractional amplitudes of the fast and slow phases showed a hyperbolic dependence on ADP concentration, yielding similar K_{AD} values of 1.3 ± 0.2 μM (Figure 5D). Thus, unlike in smooth muscle *uP*-HMM (*13*), the ADP titration data did not show any indication for heterogeneity of myosin heads, either phosphorylated or unphosphorylated, with regard to ADP affinity.

Pyrene Fluorescence Changes on acto-HMM Association. We checked for the presence of nonfunctional myosin heads in the NMIIA HMM preparations by assessing the relative change in pyrene fluorescence on the acto-HMM association reaction in the same experimental setup as we used for recording the dissociation transients (Figures 4 and 5). Usually, nonfunctional heads strongly bind to actin and are not capable of dissociation upon ATP addition. Consequently, the amplitude of the association reaction can be significantly larger than that of the dissociation reaction.

The left panel of Figure 6 compares the amplitudes of pyrene fluorescence decrease obtained on mixing 0.1 μM *tP*-HMM or *uP*-HMM (in heads) with 0.05 μM pyrene-actin (postmixing concentrations) in the presence or absence of 50 μM ADP with those of the dissociation reactions performed under similar conditions. While the amplitude data show considerable variance, it is apparent that the association and dissociation amplitudes do not systematically differ from each other. This shows that there was no significant fraction of nonfunctional heads in our HMM preparations. Interestingly, the amplitudes in *tP*-HMM ($88\% \pm 7\%$) are notably larger than in *uP*-HMM ($73\% \pm 6\%$). We also note that these NMIIA amplitudes are rather similar to those obtained by Ellison et al. (*14*) on smooth muscle HMM, whereas the amplitudes were markedly smaller in the Berger et al. study (*13*, Figure 6). In the latter work, only the dissociation amplitudes were investigated.

The NMIIA actin-binding transients were not single exponentials because the reactions did not take place in

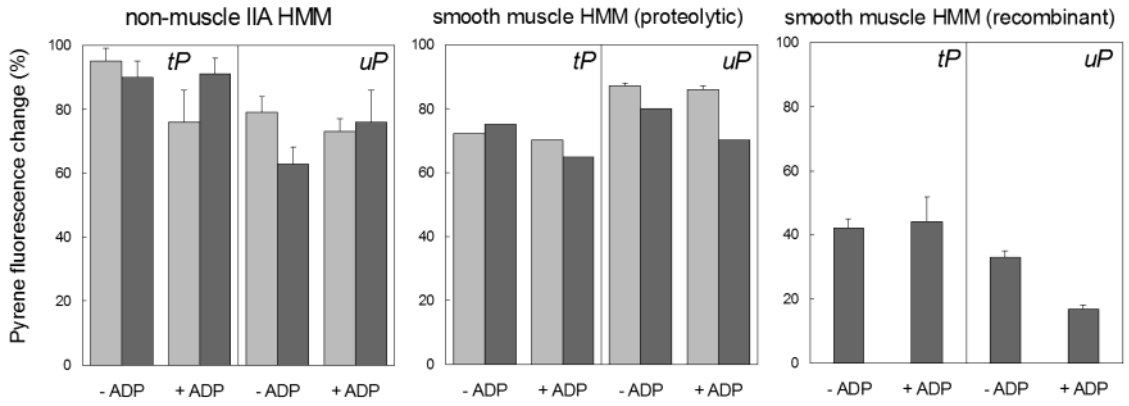

FIGURE 6: Pyrene-actin fluorescence changes on interaction with phosphorylation-regulated myosins. Relative fluorescence changes (cf. Figure 4B) on the association (light gray columns) and dissociation (dark gray columns) of different HMM constructs and pyrene-actin are shown: (left panel) NMIIA HMM (present study); (middle panel) proteolytic smooth muscle HMM (*14*); (right panel) recombinant smooth muscle myosin HMM (*13*) (only dissociation data are available). Conditions for the NMIIA HMM measurements were the same as those in Figure 3.

pseudo-first-order conditions (traces not shown). Nevertheless, the binding kinetics implied that the on-rate constant for acto-NMIIA HMM binding (k_{-A}) is in the range of 0.3−0.6 μM^{-1} s^{-1}, consistent with NMIIA S1 data (*22*).

DISCUSSION

Despite a large number of investigations, the structural basis of light chain phosphorylation-dependent regulation of myosin and the nature of the off-state is still a matter of significant controversy. It appears that an interaction between the two heads of HMM is necessary for the formation of the off-state, since one-headed fragments are constitutively active (*5*, *26*). The head−head interactions can involve contacts between the two motor domains (*6*, *7*) or the motor domain and the neck (*23*), or possibly the interaction of either of these domains with the coiled-coil tail is also necessary for regulation (*27*). It has been shown that HMM fragments with one intact head and one head lacking the motor domain are unregulated, which implies that motor domain−motor domain interactions are essential for the formation of the off-state (*6*, *7*, *26*). The structural model of Wendt et al. (*8*−*10*) strengthened this hypothesis and suggested a mechanism of inhibition whereby interactions between the actin-binding site of one motor domain and the converter region of the other impede functioning of either head. This model also provided a plausible explanation for previously inexplicable results of mutagenesis studies involving these regions of smooth muscle HMM (*28*).

Berger et al. (*13*) reported that in ADP, unphosphorylated smooth muscle HMM shows half of the pyrene fluorescence change on actin binding compared to that in the absence of ADP or in thiophosphorylated HMM, implying single-headed actin binding in these conditions. Conversely, Ellison et al. (*14*) showed identical amplitudes in thiophosphorylated and unphosphorylated HMM·ADP complexes, suggesting that both heads bind to actin in the presence of ADP regardless of the phosphorylation state. Our study demonstrates that the two heads of NMIIA HMM bind to actin in the presence of ADP and phosphorylation does not affect this property. The Berger et al. study (*13*) can be regarded as a solution kinetic implication for the asymmetrical structure seen by Wendt et al. (*8*−*10*). RLC phosphorylation, however, has been shown to primarily affect the rate constant of phosphate release from smooth muscle actomyosin (*25*, *29*) and, in line with this, our single turnover experiments with NMIIA HMM also show that reformation of the strong actin-binding state is drastically slowed by RLC dephosphorylation. Thus, it is conceivable that the Wendt et al. structure (*8*−*10*) obtained in ATP and in the absence of actin represents an intermediate that precedes the actomyosin·ADP state (e.g., myosin with ADP and phosphate bound to the active site). This is also implied by the fact that the atomic structure of smooth muscle S1 could be best fitted into the density map in the prepowerstroke conformation (*8*−*10*).

The ADP affinities of the two heads of actin-bound unphosphorylated smooth muscle HMM differ by an order of magnitude (*13*) (Table 1). This behavior is postulated to be a result of the mutual strain that the two actin-bound heads impose on each other (*13*). The smooth muscle myosin head has the interesting feature that in addition to the change in the neck ("lever arm") orientation coupled to phosphate release, the release of ADP causes an additional tilt of the neck domain in the same direction (*30*). Thus, the binding of ADP to the "leading" head (i.e., the head in the direction of the powerstroke) would reduce the strain in the HMM molecule, whereas ADP binding to the "trailing" head would increase it. This would result in different ADP affinities of the two actin-bound heads (*13*). We did not observe this phenomenon in NMIIA HMM in the present work, although relatively small (up to ∼2−3-fold) differences in the ADP dissociation constant may go undetected in the ADP titration method used. Moreover, a difference in the ADP off-rate constants of the two heads provides a possible explanation for the biphasic ADP release transients (cf. Figure 4). It remains an interesting possibility to test whether the ADP kinetics of the two heads of HMM from different isoforms can be correlated to the extent of lever arm tilt on ADP release and, in turn, the possible strain dependence of the ADP release step(s).

To date, our knowledge about the specific structural features of nonmuscle myosin II isoforms is rather limited. However, the uniquely loose coupling between actin and nucleotide binding to nonmuscle myosins (*20*, *22*, *31*) confers a great potential for the investigation of actomyosin·nucleotide ternary complexes. Furthermore, the kinetics of most steps of their ATPase cycle is slowed compared to other myosin

IIs, which is an advantageous feature in video-based applications. Due to these properties, together with their high physiological importance, nonmuscle myosin II isoforms will continue to be useful objects for the study of the myosin II mechanism.

ACKNOWLEDGMENT

We thank Dr. Fei Wang for engineering the recombinant NMIIA HMM, Estelle V. Harvey and Yue Zhang for excellent technical assistance, Olivia Henderson-Hall for providing actin for some of the experiments, and Drs. Christine R. Cremo, Robert S. Adelstein, and András Málnási-Csizmadia for helpful comments and discussions.

REFERENCES

1. Gordon, A. M., Homsher, E., and Regnier, M. (2000) Regulation of contraction in striated muscle, *Physiol. Rev. 80*, 853−924.
2. Wang, C. L. (2001) Caldesmon and smooth-muscle regulation, *Cell Biochem. Biophys. 35*, 275−288.
3. Sellers, J. R. (1999) *Myosins*, Oxford University Press, New York.
4. Bresnick, A. R. (1999) Molecular mechanisms of nonmuscle myosin-II regulation, *Curr. Opin. Cell Biol. 11*, 26−33.
5. Ikebe, M., and Hartshorne, D. J. (1985) Proteolysis of smooth muscle myosin by *Staphylococcus aureus* protease: preparation of heavy meromyosin and subfragment 1 with intact 20 000-dalton light chains, *Biochemistry 24*, 2380−2387.
6. Cremo, C. R., Sellers, J. R., and Facemyer, K. C. (1995) Two heads are required for phosphorylation-dependent regulation of smooth muscle myosin, *J. Biol. Chem. 270*, 2171−2175.
7. Cremo, C. R., Wang, F., Facemyer, K., and Sellers, J. R. (2001) Phosphorylation-dependent regulation is absent in a nonmuscle heavy meromyosin construct with one complete head and one head lacking the motor domain, *J. Biol. Chem. 276*, 41465−41472.
8. Liu, J., Wendt, T., Taylor, D., and Taylor, K. (2003) Refined model of the 10S conformation of smooth muscle myosin by cryo-electron microscopy 3D image reconstruction, *J. Mol. Biol. 329*, 963−972.
9. Wendt, T., Taylor, D., Messier, T., Trybus, K. M., and Taylor, K. A. (1999) Visualization of head−head interactions in the inhibited state of smooth muscle myosin, *J. Cell Biol. 147*, 1385−1390.
10. Wendt, T., Taylor, D., Trybus, K. M., and Taylor, K. (2001) Three-dimensional image reconstruction of dephosphorylated smooth muscle heavy meromyosin reveals asymmetry in the interaction between myosin heads and placement of subfragment 2, *Proc. Natl. Acad. Sci. U.S.A. 98*, 4361−4366.
11. Ito, K., Uyeda, T. Q., Suzuki, Y., Sutoh, K., and Yamamoto, K. (2003) Requirement of domain-domain interaction for conformational change and functional ATP hydrolysis in myosin, *J. Biol. Chem. 278*, 31049−31052.
12. Criddle, A. H., Geeves, M. A., and Jeffries, T. (1985) The use of actin labeled with N−(1-pyrenyl)iodoacetamide to study the interaction of actin with myosin subfragments and troponin/tropomyosin, *Biochem. J. 232*, 343−349.
13. Berger, C. E., Fagnant, P. M., Heizmann, S., Trybus, K. M., and Geeves, M. A. (2001) ADP binding induces an asymmetry between the heads of unphosphorylated myosin, *J. Biol. Chem. 276*, 23240−23245.
14. Ellison, P. A., DePew, Z. S., and Cremo, C. R. (2003) Both heads of tissue-derived smooth muscle heavy meromyosin bind to actin in the presence of ADP, *J. Biol. Chem. 278*, 4410−4415.
15. Wang, F., Harvey, E. V., Conti, M. A., Wei, D., and Sellers, J. R. (2000) A conserved negatively charged amino acid modulates function in human nonmuscle myosin IIA, *Biochemistry 39*, 5555−5560.
16. Spudich, J. A., and Watt, S. (1971) The regulation of rabbit skeletal muscle contraction. I. Biochemical studies of the interaction of the tropomyosin-troponin complex with actin and the proteolytic fragments of myosin, *J. Biol. Chem. 246*, 4866−4871.
17. Cooper, J. A., Walker, S. B., and Pollard, T. D. (1983) Pyrene actin: documentation of the validity of a sensitive assay for actin polymerization, *J. Muscle Res. Cell Motil. 4*, 253−262.
18. Facemyer, K. C., and Cremo, C. R. (1992) A new method to specifically label thiophosphorylatable proteins with extrinsic probes. Labeling of serine-19 of the regulatory light chain of smooth muscle myosin, *Bioconjugate Chem. 3*, 408−413.
19. Perrie, W. T., and Perry, S. V. (1970) An electrophoretic study of the low-molecular-weight components of myosin, *Biochem. J. 119*, 31−38.
20. Wang, F., Kovacs, M., Hu, A., Limouze, J., Harvey, E. V., and Sellers, J. R. (2003) Kinetic mechanism of nonmuscle myosin IIB: functional adaptations for tension generation and maintenance, *J. Biol. Chem. 278*, 27439−27448.
21. Kurzawa, S. E., and Geeves, M. A. (1996) A novel stopped-flow method for measuring the affinity of actin for myosin head fragments using microgram quantities of protein, *J. Muscle Res. Cell Motil. 17*, 669−676.
22. Kovacs, M., Wang, F., Hu, A., Zhang, Y., and Sellers, J. R. (2003) Functional divergence of human cytoplasmic myosin II: kinetic characterization of the nonmuscle IIA isoform, *J. Biol. Chem. 278*, 38132−38140.
23. Li, X. D., Saito, J., Ikebe, R., Mabuchi, K., and Ikebe, M. (2000) The interaction between the regulatory light chain domains on two heads is critical for regulation of smooth muscle myosin, *Biochemistry 39*, 2254−2260.
24. Li, X. D., and Ikebe, M. (2003) Two functional heads are required for full activation of smooth muscle myosin, *J. Biol. Chem. 278*, 29435−29441.
25. Sellers, J. R. (1985) Mechanism of the phosphorylation-dependent regulation of smooth muscle heavy meromyosin, *J. Biol. Chem. 260*, 15815−15819.
26. Sweeney, H. L., Chen, L. Q., and Trybus, K. M. (2000) Regulation of asymmetric smooth muscle myosin II molecules, *J. Biol. Chem. 275*, 41273−41277.
27. Konishi, K., Kojima, S., Katoh, T., Yazawa, M., Kato, K., Fujiwara, K., and Onishi, H. (2001) Two new modes of smooth muscle myosin regulation by the interaction between the two regulatory light chains, and by the S2 domain, *J. Biochem. (Tokyo) 129*, 365−372.
28. Trybus, K. M., Naroditskaya, V., and Sweeney, H. L. (1998) The light chain-binding domain of the smooth muscle myosin heavy chain is not the only determinant of regulation, *J. Biol. Chem. 273*, 18423−18428.
29. Sellers, J. R., Eisenberg, E., and Adelstein, R. S. (1982) The binding of smooth muscle heavy meromyosin to actin in the presence of ATP. Effect of phosphorylation, *J. Biol. Chem. 257*, 13880−13883.
30. Whittaker, M., Wilson-Kubalek, E. M., Smith, J. E., Faust, L., Milligan, R. A., and Sweeney, H. L. (1995) A 35-A movement of smooth muscle myosin on ADP release, *Nature 378*, 748−751.
31. Rosenfeld, S. S., Xing, J., Chen, L. Q., and Sweeney, H. L. (2003) Myosin IIb is unconventionally conventional, *J. Biol. Chem. 278*, 27449−27455.
32. Marston, S. B., and Taylor, E. W. (1980) Comparison of the myosin and actomyosin ATPase mechanisms of the four types of vertebrate muscles, *J. Mol. Biol. 139*, 573−600.
33. Kad, N. M., Rovner, A. S., Fagnant, P. M., Joel, P. B., Kennedy, G. G., Patlak, J. B., Warshaw, D. M., and Trybus, K. M. (2003) A mutant heterodimeric myosin with one inactive head generates maximal displacement, *J. Cell Biol. 162*, 481−488.
34. Cremo, C. R., and Geeves, M. A. (1998) Interaction of actin and ADP with the head domain of smooth muscle myosin: implications for strain-dependent ADP release in smooth muscle, *Biochemistry 37*, 1969−1978.

BI036007L